Electronic Supplementary Material (ESI) for Journal of Materials Chemistry A.

An Intelligent Anticorrosion Coating Based on pH-Responsive Smart Nanocontainers Fabricated via a Facile Method for Protection of Carbon Steel

MingDong Wang, MengYang Liu, and JiaJun Fu*[a]

Received (in XXX, XXX) Xth XXXXXXXXX 20XX, Accepted Xth XXXXXXXXX 20XX
DOI: 10.1039/b000000x

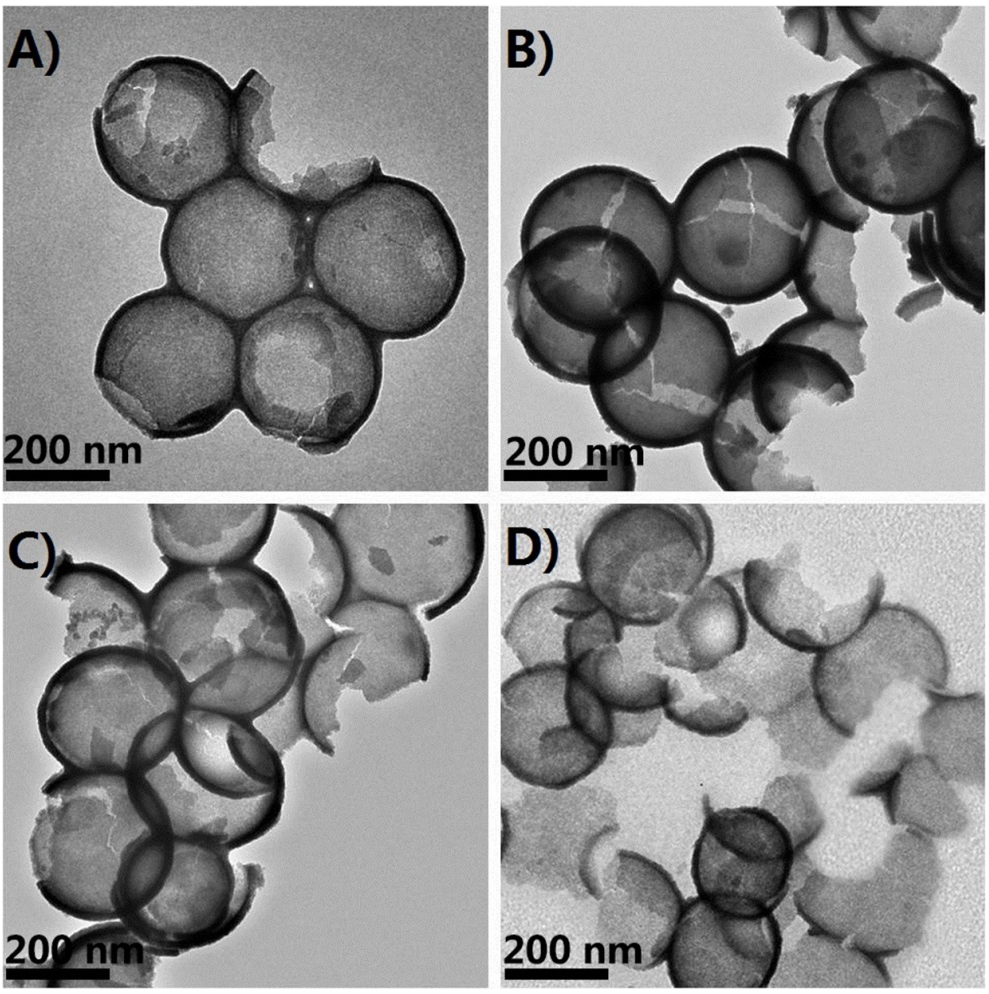

Fig. S1 TEM images of HMZSs prepared without sol-gel protection method under calcination temperature of (A) 500 ℃; (B) 600 ℃; (C) 700 ℃; and (D) 800 ℃.

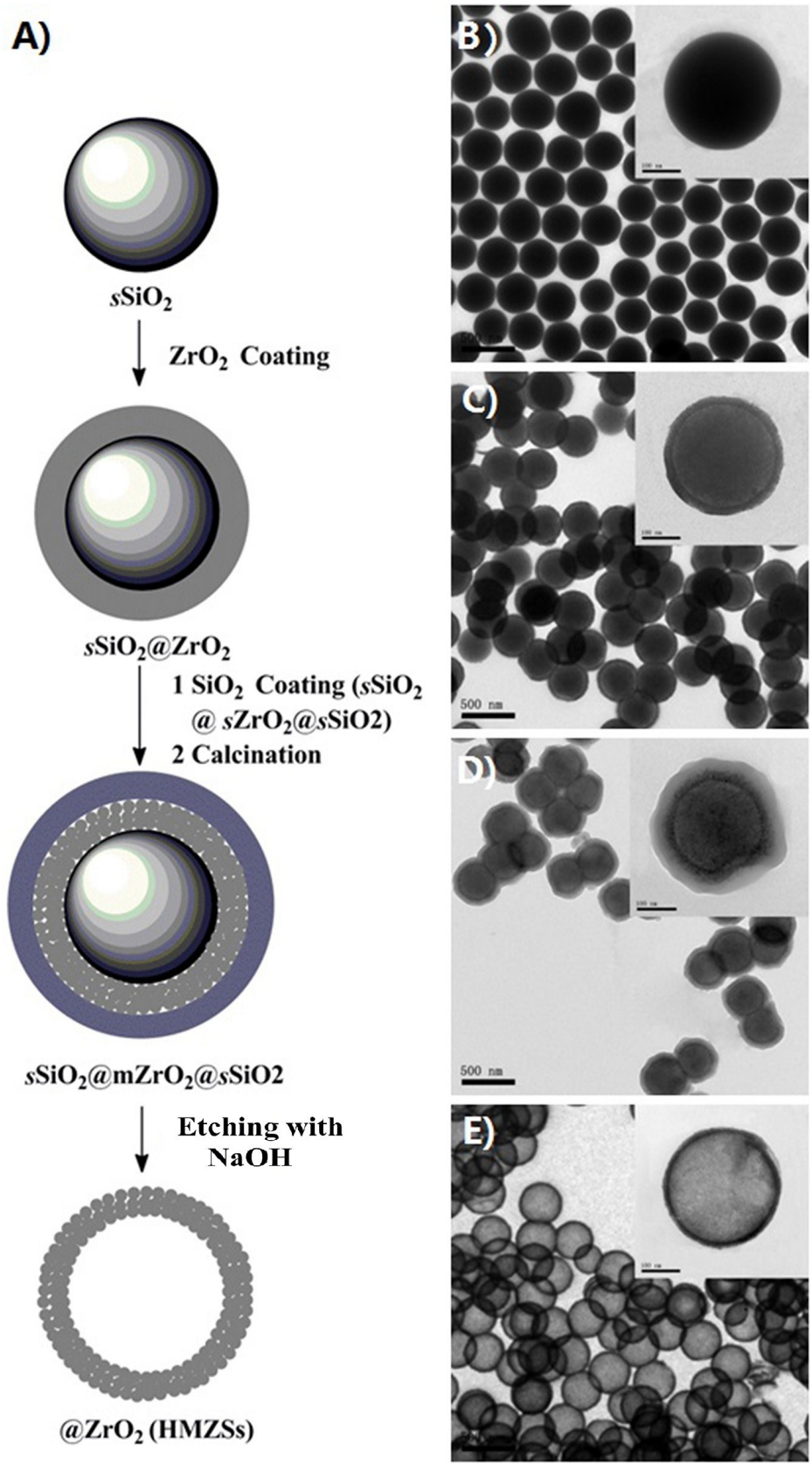

Fig. S2 (A) Schematic representation of synthetic procedure of HMZSs by sol-gel protection method; TEM images of (B) *s*SiO_2; (C) *s*SiO_2@*s*ZrO_2; (D) *s*SiO_2@*m*ZrO_2@ *s*SiO_2; (E) @*m*ZrO_2 (HMZSs).

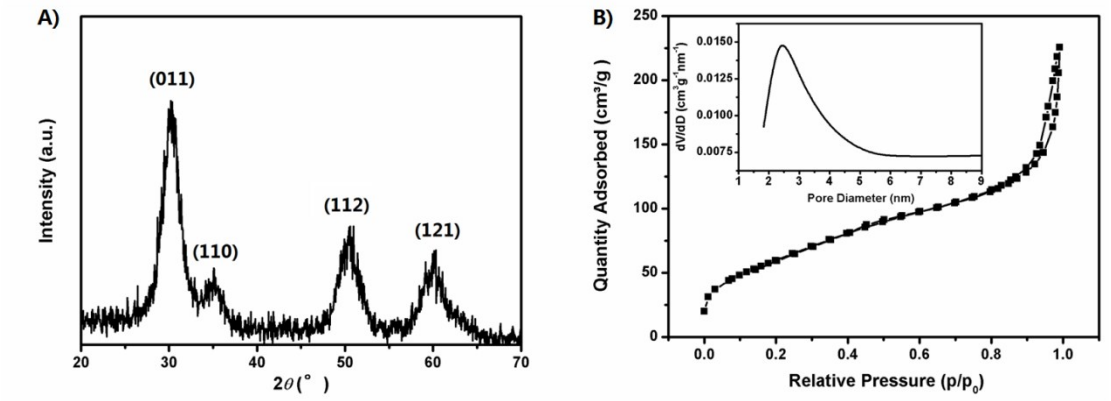

Fig. S3 (A) Powder XRD pattern for HMZSs-*d*150; **(B)** N_2 adsorption-desorption isotherm and pore-size distribution of HMZSs-*d*150.

Table S1 Physicochemical properties of the HMZSs-*d*150

Materials	Specific surface area ($m^2\ g^{-1}$)	Pore size (nm)	Pore volume ($cm^3\ g^{-1}$)
HMZSs-*d*150	225	2.40	0.27

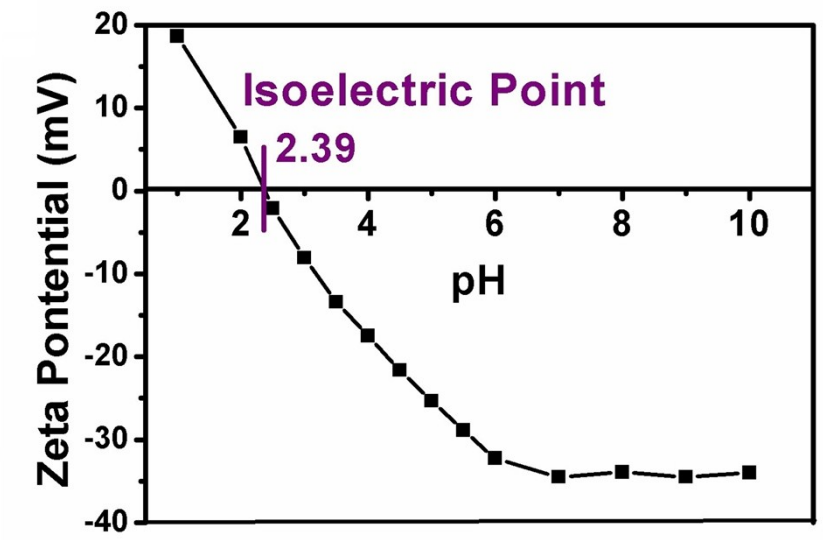

Fig. S4 Zeta potential of HMZSs-*d*300 as function of solution pH.

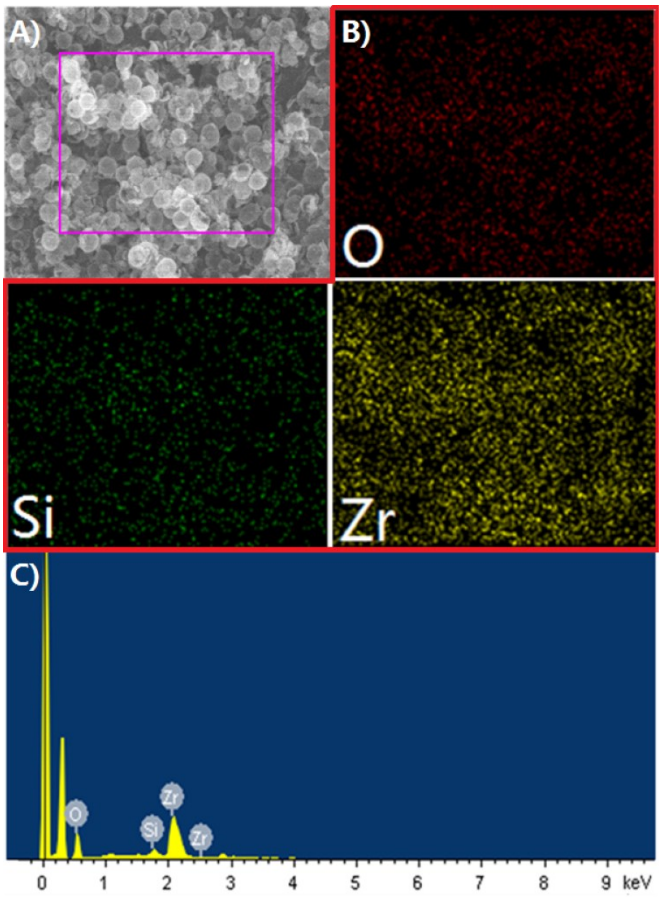

Fig. S5 (A) SEM images of HMZSs-*d*300; (B) Individual EDS maps of the marked zone for elements O, Si and Zr; and (C) EDX spectrum for HMZSs-*d*300.

It is necessary to investigate the relationship between zeta potential of HMZSs and solution pH before we begin to screen the appropriate corrosion inhibitor. Fig. S4 depicts zeta potential of HMZSs-*d*300 as function of solution pH. The isoelectric point is around pH 2.39. By analysis of EDS mapping of HMZSs-*d*300 in Fig. S5, there are still some remaining silica in the mesoporous zirconia shells after chemical etching and the occurrence of substantial silanol groups will cause the deviation of isoelectric point. As solution pH decreases from 7.0, the zeta potential of HMZSs-*d*300 pronounced increases, arising from the transition process of exterior SiO^- group to SiOH. In the other hand, when solution pH steps into the alkaline range, the pH effect on zeta potential becomes unobvious and the zeta potential keeps almost constant.

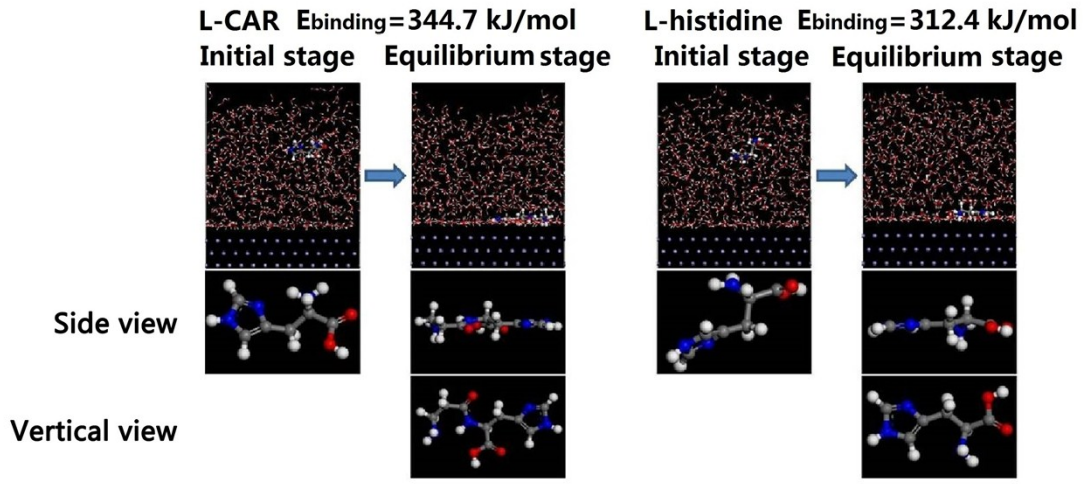

Fig. S6 Equilibrium configurations performed for L-CAR and L-histidine on Fe(110) surface in aqueous solution obtained by molecular dynamic simulations.

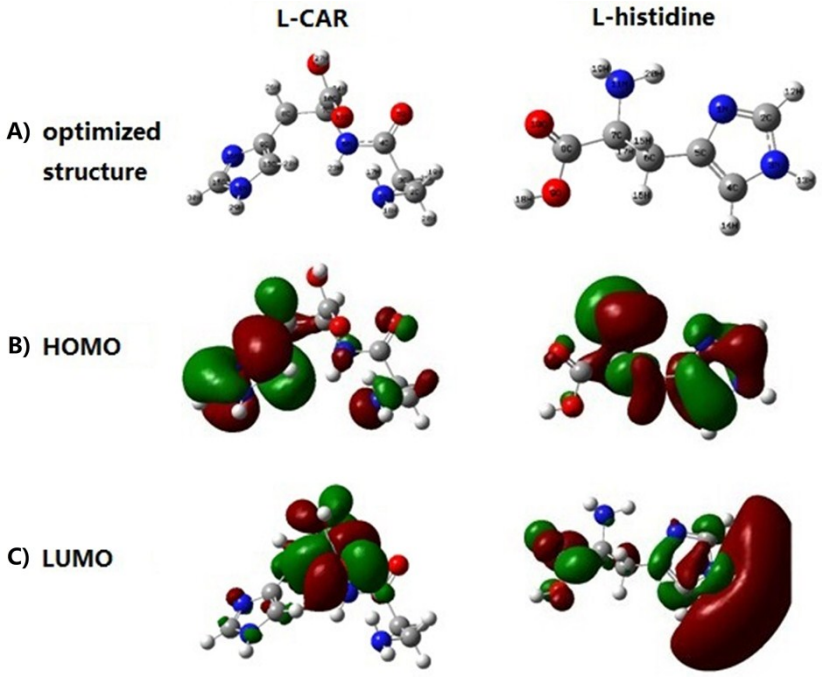

Fig. S7 (A) Optimized structure; (B) The highest occupied molecular orbital (HOMO) density; (C) The lowest unoccupied molecular orbital (LUMO) density of L-CAR and L-histidine using DFT at the B3LYP/6-31+G (d,p) basis set level.

Table S2 Calculated theoretical parameters for the compounds

Corrosion inhibitor	E_{HOMO} (eV)	E_{LUMO} (eV)	ΔE (E_{LUMO}-E_{HOMO}, eV)	Molecular Volume (cm^3 mol^{-1})
L-histidine	-0.229	-0.014	0.215	159.34

L-CAR	-0.224	-0.080	0.144	85.128

We first theoretically evaluate the qualification for L-CAR. The molecular dynamic simulations depicted in Fig. S6 demonstrate that L-CAR molecules adsorb on iron surface spontaneously through the multiple adsorption centers, such as hetero atoms (N and O) with unshared electron pairs, imidazole ring with π-electrons, and the calculated $E_{binding}$ (the binding energy between inhibitor molecule and iron surface) is 344.7 kJ mol^{-1}, even higher than that of L-histidine ($E_{binding}$=312.4 kJ mol^{-1}), evidencing its great application potential.

According to the Frontier Molecular Orbital Theory, the reactive ability of the corrosion inhibitor is considered to be closely related to their frontier molecular orbitals, HOMO and LUMO. Higher E_{HOMO} of the molecule means a higher electron-donating ability to appropriate acceptor molecules with low-energy empty molecular orbital. The lower E_{LUMO}, the more probable it is that the molecule would accept electrons. The gap between LUMO-HOMO energy levels of inhibitor molecule is another important parameter to predict inhibition efficiency. Smaller the value of ΔE (E_{LUMO}-E_{HOMO}), higher is the inhibition efficiency of the inhibitor. Based on the results presented in Table S2, compared with L-histidine, the lower E_{LUMO} and energy gap of L-CAR signify its application potential for corrosion inhibitor. The lower value of E_{LUMO} calculated by quantum chemistry suggests that L-CAR molecules are more prone to accept the electrons from d-orbital of iron to form feedback bonds than L-histidine molecules, which will enhance the adhesion strength. In addition, the higher molecular volume of L-CAR guarantees the larger coverage area on metal surface.

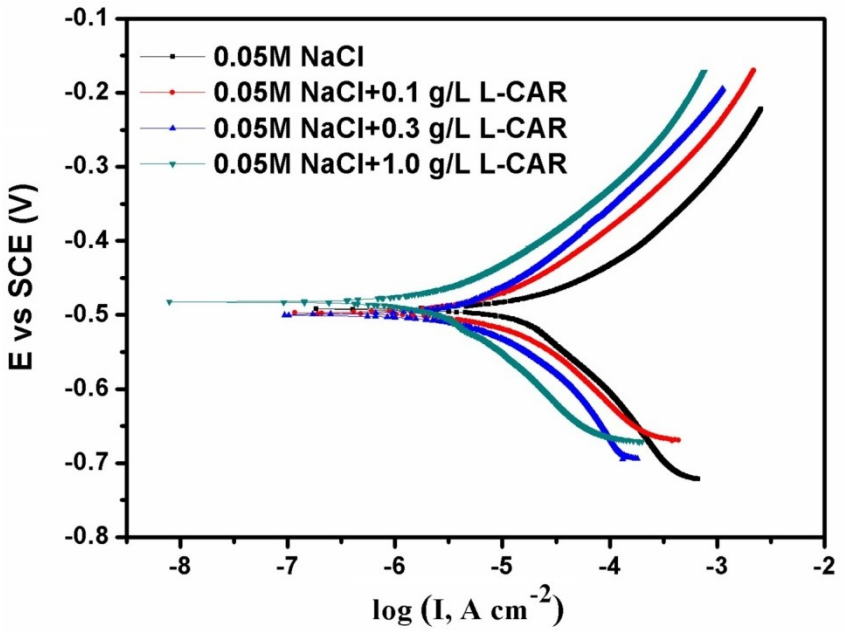

Fig. S8 Tafel plots for carbon steel in 1.0 M NaCl solution containing different concentration of L-CAR at 25 ℃.

Tafel plots for carbon steel in 1.0 M NaCl in the presence of different concentration of L-CAR at 25 ℃ are presented in Fig. S8. The corrosion parameters like corrosion potential (E_{corr}), corrosion current density (I_{corr}) calculated by extrapolation of Tafel straight line, cathodic Tafel slope (β_c), anodic Tafel slope (β_a) and percentage inhibition efficiency (η_p) are presented in Table S3. The η_p was calculated from the following equation:

$$\eta_p = \frac{I_{corr}^0 - I_{corr}}{I_{corr}^0} \times 100$$

In the above equation, where I_{corr}^0 and I_{corr} are corrosion current density in the absence and presence of inhibitor, respectively. it is found that I_{corr} values decreased considerably in presence of L-CAR and decreased with increasing inhibitor concentration while E_{corr} values remained almost unchanged ($\Delta E_{corr} < 85$ mV). These phenomena suggest that L-carnosine act as mixed type corrosion inhibitor for carbon steel in 1.0 M NaCl.[1, 2]

Table S3 Polarization parameters and corresponding inhibition efficiency for the corrosion of carbon steel in 1.0 M NaCl

Solution	Inhibitor Concentration, L-CAR mg/L	E_{corr} (mV/SCE)	I_{corr} (μA cm^{-2})	β_a (mV dec^{-1})	β_c (mV dec^{-1})	η_p (%)
1.0 M NaCl	blank	-492	11.2	99.4	160.1	—
	300	-497	2.88	93.1	164.8	74.3
	500	-500	1.43	89.7	175.2	87.2
	1000	-482	0.99	84.2	158.4	91.1

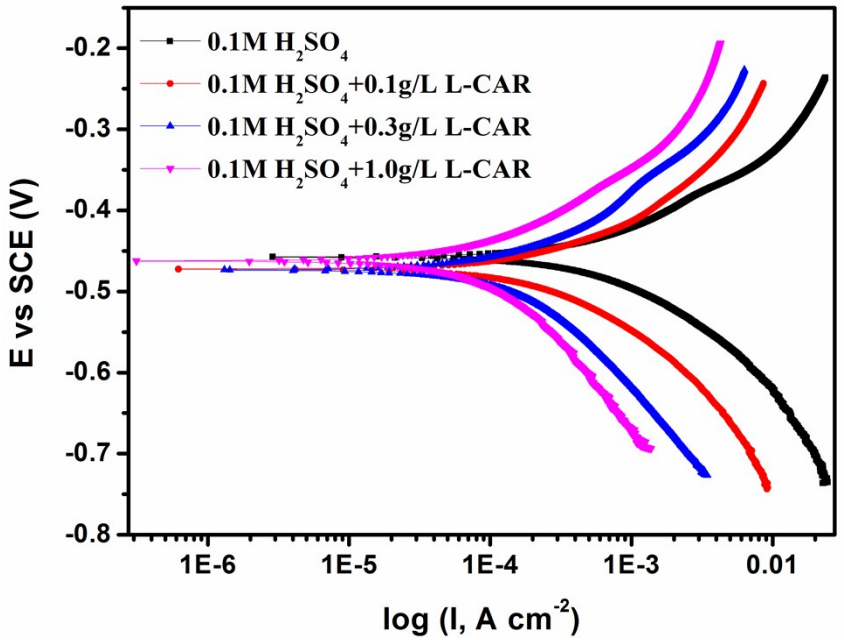

Fig. S9 Tafel plots for carbon steel in 0.1 M H_2SO_4 solution containing different concentration of L-CAR at 25 ℃.

Table S4 Polarization parameters and inhibition efficiency of L-CAR for the corrosion of carbon steel in 0.1 M H_2SO_4

Solution	Inhibitor Concentration, L-CAR mg/L	E_{corr} (mV/SCE)	I_{corr} (mA cm^{-2})	β_a (mV dec^{-1})	β_c (mV dec^{-1})	η_p (%)
0.1 M H_2SO_4	blank	-457	27.7	103.2	108.9	—
	300	-472	4.29	109.4	112.8	84.5
	500	-473	2.10	111.7	126.4	92.4

1000	-46	0.58	105.5	98.1	97.9

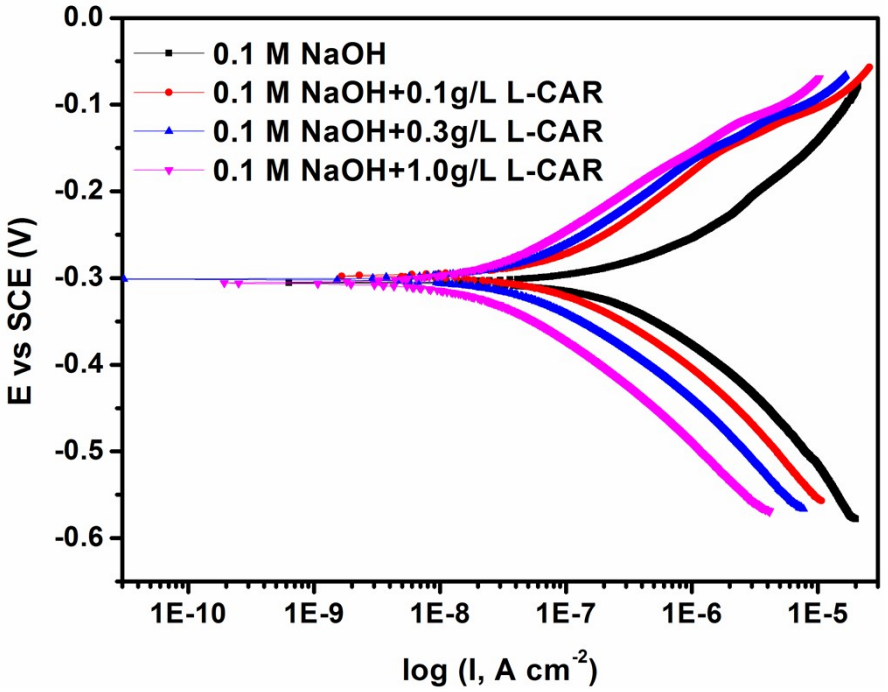

Fig. S10 Tafel plots for carbon steel in 0.1 M NaOH solution containing different concentration of L-CAR at 25 ℃.

Table S5 Polarization parameters and inhibition efficiency of L-CAR for the corrosion of carbon steel in 0.1 M NaOH.

Solution	Inhibitor Concentration, L-CAR mg/L	E_{corr} (mV/SCE)	I_{corr} (μA cm^{-2})	β_a (mV dec^{-1})	β_c (mV dec^{-1})	η_p (%)
0.1 M NaOH	blank	-305	1.4	87.2	101.4	—
	300	-297	0.29	91.2	106.2	79.2
	500	-301	0.19	97.1	115.6	86.4
	1000	-305	0.08	101.4	112.5	93.9

From Fig. S9 (Table S4) and S10 (Table S5), after addition of L-CAR, the corrosion current density decreased remarkably with increasing the concentration and the E_{corr} did not change obviously either in acidic or in alkaline solution. It can be inferred that L-CAR will show excellent corrosion inhibition performances for carbon

steel no matter in corrosive micro-anodic or micro-cathodic zones.

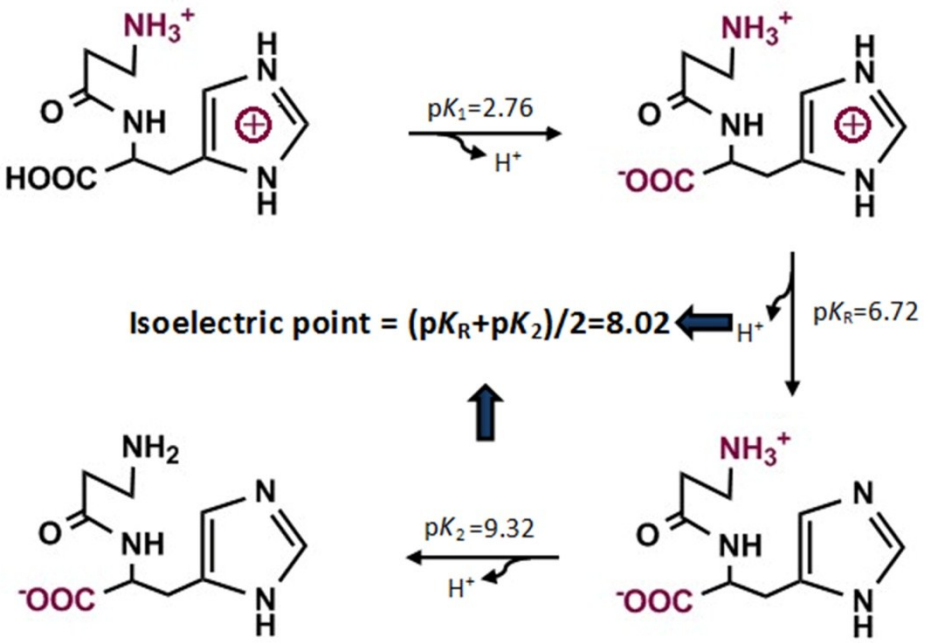

Fig. S11 Schematically representation of dissociation equation of L-CAR.

HMZSs-*d*300---inner diameter (D_1): 300 nm; external diameter (D_2): 330 nm
HMZSs-*d*150---inner diameter (D_1): 150 nm; external diameter (D_2): 210 nm

We assume the density of the mesoporous shells are the same, and denoted as ρ, then the volume of mesoporous shells are as following:

HMZSs-*d*300: $\frac{\pi D_2^3}{6}-\frac{\pi D_1^3}{6}=\frac{\pi}{6}(330^3-300^3)=1489500\pi$

HMZSs-*d*150: $\frac{\pi D_2^3}{6}-\frac{\pi D_1^3}{6}=\frac{\pi}{6}(210^3-150^3)=981000\pi$

The numbers of HMZSs-*d*300 and HMZSs-*d*150 included in unit mass are as following:

HMZSs-*d*300: $\frac{1}{1489500\times\pi\times\rho}$

HMZSs-*d*150: $\frac{1}{981000\times\pi\times\rho}$

The hollow volumes of HMZSs-*d*300 and HMZSs-*d*150 per nanospheres are as following:

HMZSs-*d*300: $\frac{\pi}{6}\times300^3=4500000\pi$

HMZSs-*d*150: $\frac{\pi}{6}\times150^3=562500\pi$

Therefore, the total hollow volumes of HMZSs-*d*300 and HMZSs-*d*150 in unit mass are as following:

HMZSs-*d*300: $\frac{1}{1489500\times\pi\times\rho}\times4500000\pi=\frac{3.021}{\rho}$

HMZSs-*d*150: $\frac{1}{981000\times\pi\times\rho}\times562500\pi=\frac{0.573}{\rho}$

If we ignore the small proportion of adsorbed L-CAR in mesoporous shells, the ratio of hollow cavity volume between HMZSs-*d*300 and HMZSs-*d*150 is about 5.27.

Scheme S1. Theoretical calculation processes of ideal adsorption capacity for HZMSs-*d*300 and HZMSs-*d*150.

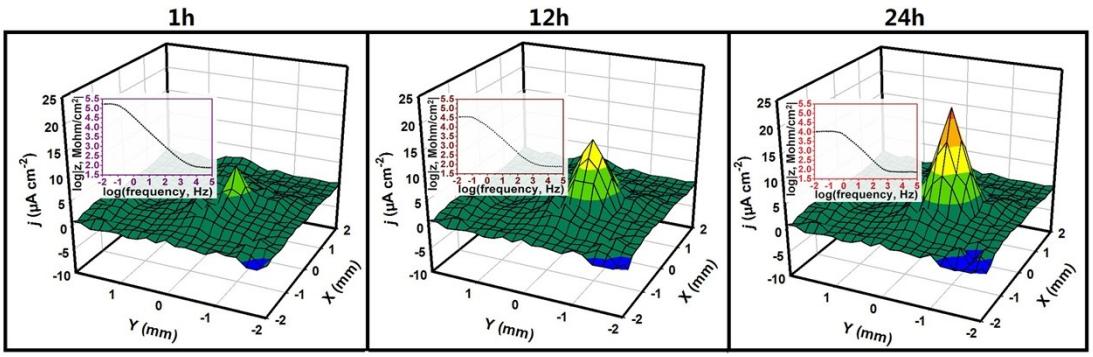

Fig. S12 SVET maps of the ionic current measured above the scratched surface of carbon steel species coated with the unloaded HMZSs-*d*300 incorporated epoxy coating at different time after immersion in 0.02 M NaCl. The inset graphs represent the corresponding Bode plots measured in 0.1 M NaCl.

Theoretical Assessment of Inhibition Performances of L-CAR:

Quantum chemical calculations were conducted with Gaussian 03 program. The molecular structures of corrosion inhibitors were geometrically optimized by the density functional theory (DFT)/B3LYP method with the basis set 6-31G+ (d, p). The molecular dynamics simulations (MD) were performed using the Materials Studio software from Accelrys Inc. Fe (110) surface was chosen for the simulation study due to its stable property. The MD simulation was carried out in a simulation box (29 Å×29 Å×67 Å) with periodic boundary conditions in order to model a representative part of an interface devoid of any arbitrary bound effects. The MD simulation was performed under 298 K, NVT ensemble, with a time step of 0.1 fs and simulation time of 50 ps using DISCOVERY module and COMPASS force field. During the process of simulations, all the atoms in Fe (110) surface were kept "frozen", and the one L-CAR molecule and 600 water molecules were allowed to interact with the iron surface freely. The interaction energy between the inhibitor molecule and the Fe (110) surface was calculated as following:

$$E_{\text{Fe-inhibitor}} = E_{\text{total}} - (E_{\text{surface}} + E_{\text{inhibitor}})$$

In above equation, $E_{\text{inhibitor}}$, E_{surface} and E_{total} represent the energies of an inhibitor molecule, the metal surface without inhibitor adsorption, and the total system containing an inhibitor molecule and metal surface, respectively. The binding energy between the inhibitor molecule and Fe (110) surface is the negative value of the

interaction energy, $E_{\text{binding}} = -E_{\text{Fe-inhibitor}}$.

References:

1. Khaled, F. Corrosion control of copper in nitric acid solutions using some amino acids-A combined experimental and theoretical study. *Corros. Sci.* **2010**, *52*, 3225.

2. Nataraja, S. E.; Venkatesha, T. V.; Manjunatha, K.; Poojary, B.; Pavithra, M. K.; Tandon, H. C. Inhibition of the corrosion of steel in hydrochloric acid solution by some organic molecules containing the methylthiophenyl moiety. *Corros. Sci.* **2011**, *53*, 2651.